Tuning On–Off Current Ratio and Field-Effect Mobility in a MoS_2–Graphene Heterostructure *via* Schottky Barrier Modulation

Chih-Jen Shih, Qing Hua Wang, Youngwoo Son, Zhong Jin, Daniel Blankschtein, and Michael S. Strano*

Department of Chemical Engineering, Massachusetts Institute of Technology, Cambridge, Massachusetts 02139, United States

ABSTRACT Field-effect transistor (FET) devices composed of a MoS_2–graphene heterostructure can combine the advantages of high carrier mobility in graphene with the permanent band gap of MoS_2 for digital applications. Herein, we investigate the electron transfer, photoluminescence, and gate-controlled carrier transport in such a heterostructure. We show that the junction is a Schottky barrier, whose height can be artificially controlled by gating or doping graphene. When the applied gate voltage (or the doping level) is zero, the photoexcited electron–hole pairs in monolayer MoS_2 can be split by the heterojunction, significantly reducing the photoluminescence. By applying negative gate voltage (or *p*-doping) in graphene, the interlayer impedance formed between MoS_2 and graphene exhibits an 100-fold increase. For the first time, we show that the gate-controlled interlayer Schottky impedance can be utilized to modulate carrier transport in graphene, significantly depleting the hole transport, but preserving the electron transport. Accordingly, we demonstrate a new type of FET device, which enables a controllable transition from NMOS digital to bipolar characteristics. In the NMOS digital regime, we report a very high room temperature on/off current ratio ($I_{ON}/I_{OFF} \sim 36$) in comparison to graphene-based FET devices without sacrificing the field-effect electron mobilities in graphene. By engineering the source/drain contact area, we further estimate that a higher value of I_{ON}/I_{OFF} up to 100 can be obtained in the device architecture considered. The device architecture presented here may enable semiconducting behavior in graphene for digital and analogue electronics.

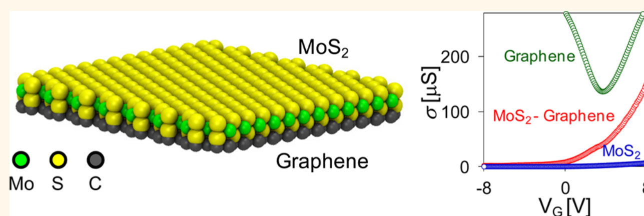

KEYWORDS: field-effect mobility · MoS_2–graphene · Schottky barrier modulation · field-effect transistor devices

The recent development of nanoelectronics using two-dimensional (2D) materials[1,2] has demonstrated potential toward further miniaturization beyond Moore's law,[3] as well as a high-mobility solution in the emerging fields of large-area, flexible, and low-cost electronics.[2,4] The 2D material that has received the most attention is graphene, a one-atom-thick, two-dimensional sheet of sp^2-hybridized carbon.[5] Graphene itself is a semimetal with zero band gap, while its ultrahigh carrier mobility[6−8] can provide superior current drive under low voltage bias. Recent progress in the production of large-area graphene using chemical vapor deposition (CVD)[9] has further shed light on engineering the material for wafer-scale integration.[10] Nevertheless, for most electronic applications, graphene requires advanced methods to open a significant transport band gap without sacrificing its intrinsic electron and hole mobilities.[11] Despite considerable research effort toward band gap engineering of graphene, most of these methods suffer from a band gap *versus* mobility trade-off[11] or heightened sensitivity to disorder.[12,13] For example, the graphene nanoribbon (GNR) devices can potentially open a band gap up to ~0.5 eV, enabling a high on–off current ratio. However, in order to achieve a narrow ribbon width with edge structure control, atomically precise processing is required, which remains a significant challenge for large-scale production.[11] Another candidate, dual-gate bilayer graphene (BLG) structure, is potentially more mass-producible; nevertheless, it is very difficult to control the location of the charge neutrality point (CNP), since in order to open a band gap,

* Address correspondence to strano@mit.edu.

Received for review February 3, 2014 and accepted May 13, 2014.

Published online May 13, 2014
10.1021/nn500676t

© 2014 American Chemical Society

one needs to apply a large electric displacement field, which often moves the CNP far from zero.[11] On the other hand, molybdenum disulfide (MoS_2), a 2D semiconductor material, is attractive as a potential complement to graphene. It possesses an indirect band gap (of 1.2 eV as a multilayer and a direct band gap of 1.8 eV as a monolayer)[14,15] that has enabled digital electronic components[3,16−24] and circuits[2] on top. However, MoS_2 itself may not be promising for high-performance digital applications because of its relatively heavier electronic mass and low carrier mobility (∼1−50 cm^2/(V s)).[25,26] A material or structure that combines the high mobility of graphene and the band gap of MoS_2 would be ideal.

Very recently, a new approach to graphene-based transport devices was advanced. Rather than directly engineering the graphene layers to open a bandgap, a graphene-based heterostructure is formed with a perpendicular transport barrier between graphene and semiconducting[27,28] or ultrathin insulating[29] materials. For example, the Schottky barrier formed between graphene and silicon can be tuned to be as high as 0.2 eV by adjusting the gate voltage, leading to a large modulation of the perpendicular transport current.[27] The impedance of atomically thin hBN between two graphene sheets can also provide a significant barrier for tunneling transport.[29] The current forms of the perpendicular device architectures, nevertheless, can only provide a current density of ∼1 to 1000 A/cm^2,[27−29] suggesting that to enable a typical current drive (∼ mA), one would require ∼100 to 100 000 μm^2 device area, which is, effectively, equivalent to a low-mobility field-effect transistor. In other words, the most important benefit for graphene-based devices, the high carrier mobility, which corresponds to the "in-plane" electronic transport, is actually wasted. Moreover, the new concepts often involve atomic-level, precision processing, which remains a significant challenge for mass production.

In this report, we study charge transfer, photoluminescence (PL), and gate-controlled electronic transport in MoS_2−graphene heterostructures. We first characterize the heterostructures using conductive atomic force microscopy (c-AFM) and Raman spectroscopy, showing that there is a significant charge transfer between the two atomic materials. In addition, the PL intensity for the heterostructure of monolayer MoS_2 and graphene is about 20% quenched compared to that of monolayer MoS_2 alone. We then fabricate field-effect transistor (FET) devices on the MoS_2−graphene heterostructures and investigate their transport characteristics. Under negative gate bias, there exists a strong interlayer impedance due to the formation of an atomic Schottky barrier, such that the hole transport in graphene is partially, or completely, depleted. Under different drain bias, we demonstrate a new type of FET device, which enables a controllable transition from NMOS digital to bipolar characteristics. In the NMOS digital regime, we show that the on/off current ratio can be tuned to be as high as ∼100, without sacrificing the field-effect mobility of graphene at room temperature. To our knowledge, this is the highest on/off current ratio ever reported in graphene-based FET devices. Accordingly, this study opens a window toward graphene-based digital and analogue electronics.

RESULTS AND DISCUSSION

Electron Transfer and Photoluminescence. In order to study electron transfer and PL in MoS_2−graphene heterostructures without applying transverse electric fields, we fabricated the stacked atomic layers by the micromechanical exfoliation of MoS_2 crystals onto a SiO_2 substrate, followed by transferring a piece of monolayer, CVD-synthesized graphene onto the surface. The cross-sectional view, optical microscope image and topographical sketch of a representative graphene-coated MoS_2 crystal are shown in Figure 1a, b,c, respectively. The regions associated with monolayer (1), trilayer (3), and bulk MoS_2 are identified using Raman spectroscopy (see Figure 1f) and labeled in Figure 1c. It is noteworthy that there is a tear formed unintentionally in graphene during the transfer process, allowing us to compare the behavior of MoS_2 with and without interacting with graphene. The technical details of the graphene synthesis and transfer are described in the Supporting Information Section S1.

First, c-AFM is used to characterize the MoS_2−graphene heterostructure (see Supporting Information Section S2).[30] Figure 1a shows the schematic diagram of the electrical setup for the system, which enables us to simultaneously measure spatial topography and current through a diamond-coated tip. In the heterostructure considered here, since graphene is basically coated on the entire surface, the two-terminal measurement essentially provides local information about the relative conductivity of graphene in contact with different materials, including MoS_2 and SiO_2. Figure 1d, e shows the height and current profiles for the heterostructure, respectively. Along with Figure 1a−c, it appears that graphene becomes less conductive when in contact with MoS_2, and there is no obvious dependence on the thickness of MoS_2. Since the interactions between graphene and MoS_2 are van-der-Waals-like,[31] it is believed that the electronic structure of graphene is not significantly influenced by the underlying MoS_2. Therefore, the reduction in the conductivity of graphene implies that the Fermi level position, E_F, for graphene lying on MoS_2 is closer to the Dirac point, E_{Dirac}, than that on SiO_2, such that the density of states around the Fermi level is significantly reduced because of the cone-shaped band structure of graphene (see Figure 1e).[5]

To further justify the Fermi level hypothesis, Raman spectroscopy was used to characterize the

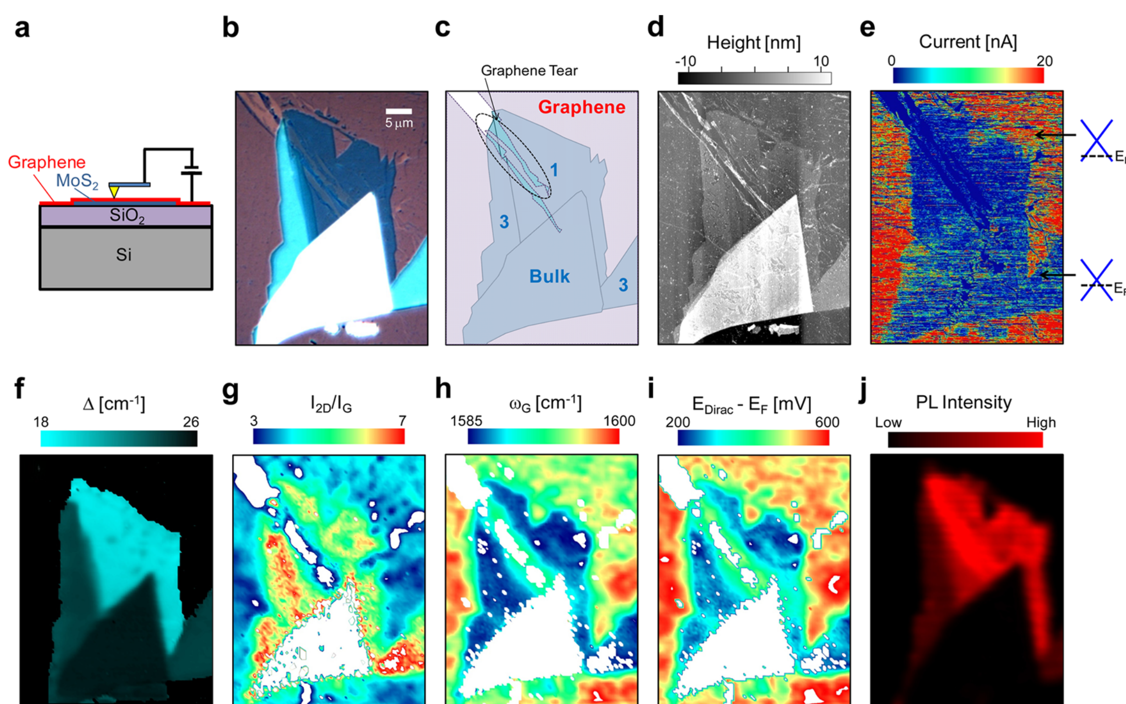

Figure 1. Characterization of electron transfer and photoluminescence in an MoS_2−graphene heterostructure. (a) Cross-sectional view and measuring setup of our c-AFM system, (b) optical microscope image, and (c) topographical diagram for a CVD graphene-coated MoS_2 single crystal. The regions associated with monolayer (1), trilayer (3), and bulk MoS_2 are identified using Raman spectroscopy and labeled. (d) Measured topographical height and (e) current profiles using our c-AFM system (V_{Sample} = 0.5 V). The Fermi level positions of graphene associated with the regions lying on SiO_2 (top) and MoS_2 (bottom) are also shown. Spatial Raman maps for (f) Δ, (g) I_{2D}/I_G, (h) ω_G, (i) the calculated ($E_{Dirac} - E_F$), and (j) PL intensity for the MoS_2−graphene heterostructure considered.

MoS_2−graphene heterostructure. Raman spectroscopy has demonstrated its versatility in 2D materials research.[1,32] Here, in particular, since the Raman spectrum for graphene is very sensitive to the doping level,[33,34] it allows us to resolve the Fermi level position locally. Accordingly, thousands of Raman spectra were taken to cover the entire sample (see Figure S1, Supporting Information). All prominent peaks were fitted with Lorentzian functions to extract peak position (ω), full width at half-maximum (fwhm), and integrated intensity (I). The technical details of Raman spectroscopy and parameter extraction are described in Supporting Information Section S2. The spatial Raman maps for several important peak parameters are shown in Figure 1f−i and Figure S3 (Supporting Information).

For the region of MoS_2 crystal, the two signature peaks of MoS_2, the E^1_{2G} and A_{1G} peaks, were clearly observed (see Figure S2, Supporting Information). By reducing the number of MoS_2 layers, the frequency for the E^1_{2G} peak increases and that for the A_{1G} peak decreases,[35] and the frequency difference between the two peaks, Δ, allows us to quantify the number of MoS_2 layers.[35] Figure 1f shows the spatial Raman map of Δ. The regions associated with monolayer (1), trilayer (3), and bulk MoS_2 (see Figure 1c) are clearly identified because of the quantized nature of Δ.[35] On the other hand, the Raman spectrum for monolayer graphene consists of two prominent peaks, the G and $2D$ peaks, positioned at around 1580 and 2640 cm^{-1}, respectively.[36] For each spectrum, the doping carrier density (n) and the Fermi level position relative to the Dirac point ($E_{Dirac} - E_F$) of graphene are calculated on the basis of the position of the G and $2D$ peaks.[33] Specifically, the G peak position upshifts monotonically by increasing the doping level in graphene ($|E_{Dirac} - E_F| > 0$), while $2D$ peak position upshifts when p-doping ($(E_{Dirac} - E_F) < 0$) and downshifts when n-doping ($(E_{Dirac} - E_F) < 0$).[33] Following the empirical trajectories,[33] the obtained spectroscopic parameters allow us to quantify the Fermi level position, as well as the carrier density, n, locally.

Figure 1g−i shows the spatial Raman maps of I_{2D}/I_G, ω_G, and the calculated ($E_{Dirac} - E_F$) of graphene, respectively. Additional spatial Raman maps can be found in Figure S3 (Supporting Information). We notice that the two important peaks of graphene, however, become obscure on thick (>3 layer) MoS_2 flakes, because of the broadening PL response and reduced light transmittance of thick MoS_2 flakes. For all the spectra of graphene, the $2D$ peak can be described by a single Lorentzian function with fwhm of 26−28 cm^{-1}, suggesting that the graphene is monolayer.[32] The average positions of the G and $2D$ peaks for the graphene on SiO_2 ($\varpi_G = 1593$ cm^{-1} and $\varpi_{2D} = 2648$ cm^{-1}), as well as their intensity ratio ($I_{2D}/I_G = 4$), indicate that graphene

is heavily hole-doped with a carrier density $n = -2 \times 10^{13}$, corresponding to ($E_{Dirac} - E_F$) = 550 mV. On the other hand, the spectroscopic parameters for graphene in contact with MoS_2 ($\varpi_G \sim 1586\ cm^{-1}$, $\varpi_{2D} = 2644\ cm^{-1}$, and $I_{2D}/I_G = 6$) suggest that graphene is hole-doped with $n = -1 \times 10^{13}$, corresponding to ($E_{Dirac} - E_F$) = 250 mV. It appears that additional electrons are transferred from MoS_2 to graphene such that graphene is "counter-doped" by the underlying MoS_2 flake, or in other words, that MoS_2 is hole-doped by graphene. The upshift of Fermi level position in graphene, as well as its independence on layer number of MoS_2, confirms our finding in the c-AFM characterization (see Figure 1e).

Monolayer MoS_2 is a semiconductor with a direct band gap of ~1.8 eV, which is optically active in the visible light range, generating strong photoluminescence (PL).[14] Since PL essentially describes the process of light emission after the absorption of photons, the quantum yield for the recombination of the hot carriers across the band gap plays an important role. A representative PL spectrum for monolayer MoS_2 under a green light excitation (λ = 532 nm) is shown in Figure S4 (Supporting Information), and the PL intensity for each spectrum is calculated by integrating the emitted PL counts with respect to the wavelength from 532 to 720 nm. Figure 1j shows the spatial map of PL intensity. As expected, because of the transition from indirect to direct band gap, the PL intensity in monolayer MoS_2 is much higher than that in trilayer and bulk MoS_2. For the region of monolayer MoS_2, since there is a tear formed in graphene (see Figure 1b,c), we can quantify the effect of graphene on the change of PL in monolayer MoS_2, as shown in Figure 1j. We found that the integrated PL intensity, as well as the maximum intensity (at ~680 nm, corresponding to photon energy of ~1.82 eV, see also Figure S4, Supporting Information), is considerably quenched by 20% when in contact with graphene. Apparently, the observed changes in PL intensity are not caused by the change of E_F in MoS_2, since the change in the carrier density in MoS_2 ($\Delta n \sim -1 \times 10^{13}\ cm^{-2}$) is only associated with a downshift of Fermi level energy $\Delta E_F = \pi\hbar^2\ \Delta n/m_e \sim -70$ meV, where $m_e \sim 0.35m_0$ is the effective electron mass in MoS_2, and this shift is negligible compared to the dominant photon energy (~1.82 eV).[37] Considering the fact that graphene is about 98% transparent to visible light,[38] one possible mechanism for the observed quenching is the exciton splitting by the built-in potential formed between monolayer MoS_2 and monolayer graphene.[39] Specifically, exciton splitting occurs by injecting the photogenerated electrons from the conduction band of MoS_2 to graphene,[40] while the photogenerated holes in the valence band of MoS_2 cannot diffuse to graphene because of the built-in potential formed in the heterojunction.[39] Therefore, the recombination events, as well as the resulting photoluminescence, are significantly reduced. In our opinion, the indirect evidence may imply that the atomically thin junction can be utilized to split the photoexcited electron–hole pairs in monolayer MoS_2, which may be useful to realize transition metal dichalcogenides-based photovoltaics.[39] It is noteworthy that, very recently, Buscema *et al.* have observed that the PL intensity of monolayer MoS_2 strongly depends on the choice of underlying substrate.[41] However, we are not certain if it is directly related to what we have observed here. Moreover, different mechanisms, including strains and interfacial interactions, may involve as well. In order to justify our hypothesis, a more detailed investigation of optoelectronic response in the junction under electric fields is underway and will be published in our subsequent report.

Gate-Controlled Interlayer Impedance. For the monolayer MoS_2–monolayer graphene heterojunction considered in Figure 1, since MoS_2 is essentially an *n*-type (electron-rich) semiconductor, while the as-prepared graphene is significantly hole-doped (electron-depleted), it is not surprising that free electrons of $n \sim 1 \times 10^{13}\ cm^{-2}$ are transferred from MoS_2 to graphene. Quantitatively, since the work function for pristine graphene, $\Phi_{G,i}$, is 4.9 eV,[42] and our as-prepared CVD graphene is heavily hole-doped (($E_{Dirac} - E_F$) ~ 550 mV), the work function for the as-prepared graphene is estimated to be ~5.45 eV. On the other hand, monolayer MoS_2 has an electron affinity of 4.0 eV,[15] and considering its band gap (E_G ~ 1.8 eV)[14] and *n*-doped nature,[14] the work function of MoS_2, Φ_{MoS_2}, is smaller than 4.9 eV. Therefore, when MoS_2 and graphene are in contact, there exists a driving force (>0.55 V) that transfers electrons from MoS_2 to graphene. According to our calculations in the last section, in order to align their E_F for all the regions, the entire band structure for graphene in the heterostructure downshifts ~300 mV, and that for MoS_2 upshifts ~70 mV, contributing to a modified work function, Φ_G ~ 5.15 eV, for graphene in the heterostructure. Consequently, if we assume that MoS_2 behaves like a bulk semiconductor, since $\Phi_G > \Phi_{MoS_2}$, for the hot electrons generated and transferred from MoS_2 to graphene after photoexcitation, there is a Schottky barrier (SB)[43] built at the MoS_2–graphene interface, corresponding to a barrier height of $\Phi_{SB} = \Phi_G - \Phi_{MoS_2} > (5.15-4.9) = 0.25$ eV. The resulting built-in potential, as discussed in the last section, can therefore split the photoexcited electron–hole pairs, reducing the PL of monolayer MoS_2. The same analysis also applies for the system of multilayer MoS_2. The schematic diagram for the band structure of a MoS_2–graphene heterostructure, as well as those in the bare graphene and bare MoS_2 regions on the same sample, are shown in Figure 2a. It is noteworthy that we have chosen to represent the MoS_2 using a continuous band model in the following analysis, applicable to bulk MoS_2. This model allows for the presence of an

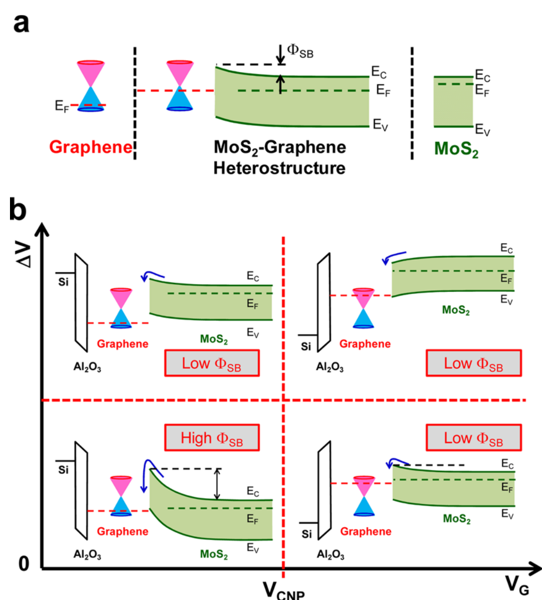

Figure 2. Formation of atomic Schottky barrier at an MoS_2–graphene interface. (a) Schematic band diagram for a MoS_2–graphene heterojunction without applying electric fields. From estimates in Figure 1, graphene bands downshift 300 eV, while MoS_2 bands deflect upward 70 mV, yielding a modified work function of ~5.15 eV and a ~0.25 eV Schottky barrier at the MoS_2/graphene interface. The L1 to L4 denote the layer number considered in the MoS_2–graphene heterostructure. (b) Modulation of the work function at the MoS_2–graphene interface. Schematic band diagrams for the MoS_2–graphene heterojunction, which has graphene in touch with gate dielectrics, as a function of gate voltage, V_G, and the voltage difference between MoS_2 and graphene, ΔV. When $V_G < V_{CNP}$ where the latter is the charge neutrality point in graphene, and ΔV is small, graphene becomes more hole doped, boosting the heterostructure work function, with the opposite occurring as $V_G > V_{CNP}$. When ΔV is large, the barrier is reduced by ΔV or becomes Ohmic, enhancing the on–off ratio of the device.

interfacial state between the graphene and MoS_2 that provides for a barrier that can be modulated as the number of MoS_2 layers becomes discretized down to monolayer.

The above analyses further imply that if we can modulate the work function of graphene in the MoS_2–graphene heterostructure using electrostatic gating, the Schottky barrier height becomes externally tunable as well. Therefore, if we consider a MoS_2–graphene heterostructure, which has graphene in contact with the gate dielectrics (100 nm Al_2O_3 considered here), the ideal schematic band diagrams as a function of gate voltage, V_G, and the voltage difference between MoS_2 and graphene, ΔV, are schematically shown in Figure 2b. Specifically, we first consider the cases of small ΔV, which is associated with aligned E_F in MoS_2 and graphene. When $V_G < V_{CNP}$, where V_{CNP} is the charge neutrality point (CNP) of graphene, graphene becomes more hole-doped, such that the work function of graphene in the heterostructure, $\Phi_{G,p}$, is boosted, resulting in a higher Schottky barrier height $\Phi_{SB} = \Phi_{G,p} - \Phi_{MoS_2}$. On the other hand, positive gate bias ($V_G > V_{CNP}$) induces electrons in graphene and decreases graphene's work function, $\Phi_{G,n}$, such that the Schottky barrier height between graphene and MoS_2, $\Phi_{SB} = \Phi_{G,n} - \Phi_{MoS_2}$, is lowered. For the cases of high ΔV, the Schottky barrier is lowered by ΔV, inducing a reduced Schottky barrier or even becoming Ohmic ($\Phi_{SB} < 0$). More importantly, if the Schottky barrier works effectively, by coating a layer of MoS_2 on graphene, the gate-controlled interlayer impedance may be useful to reduce the "off current" in the field-effect transport of graphene.

It is noteworthy that for the system considered in Figure 2b, Φ_{MoS_2} is assumed to be independent of V_G because of the following reasons: (i) Gating in MoS_2 is much less efficient relative to graphene because of the large effective electron mass in MoS_2 (see the related discussion in the last section). (ii) The electric field transmitted to MoS_2 is significantly screened by the underlying graphene, which is in contact with the gate dielectrics, since graphene is a semimetal, whose electron density is extremely high (*i.e.*, graphene behaves like a continuous metal). More importantly, it is presumed that the gate-controlled Schottky barrier can be utilized to modulate splitting of photoexcited electron–hole pairs in MoS_2 (see Figure 1j) as well. In other words, by applying a gate bias $V_G < V_{CNP}$ (or *p*-doping) in graphene, one would expect to reduce the exciton recombination, and enhance the resulting photon-to-exciton quantum efficiency in MoS_2. The optoelectronic response of the atomic Schottky barrier under electrical gating is beyond the scope of this manuscript and will be presented in our subsequent reports.

With the above analyses in mind, for the first time, we propose a new FET architecture composed of graphene and gate-controlled MoS_2–graphene Schottky barriers, which is illustrated in Figure 3a. Specifically, a *p*-doped silicon wafer was coated in 100 nm Al_2O_3 using atomic layer deposition (ALD). A piece of monolayer, CVD-synthesized graphene was then transferred onto the substrate (Figure 3a(i)), followed by the mechanical exfoliation of multilayer MoS_2 single crystals onto graphene (Figure 3a(ii)). The area of graphene exposed to air was then removed using reactive ion etching in oxygen plasma (Figure 3a(iii)), while the graphene underlying MoS_2 was preserved because of a much slower etch rate of MoS_2, allowing it to act as an etch mask for the graphene. Finally, the source (S) and drain (D) contacts were patterned onto the etched stack using ultraviolet photolithography, followed by the deposition of Ti/Au contact electrodes (Figure 3a(iv)). Transport characteristics of the heterostructure were determined in a vacuum at room temperature (RT). The detailed fabrication and characterization methods are described in Supporting Information Section S3.

Since the electronic transport for MoS_2 and graphene in the channel region are typically independent, the electronic transport in the heterostructure can be

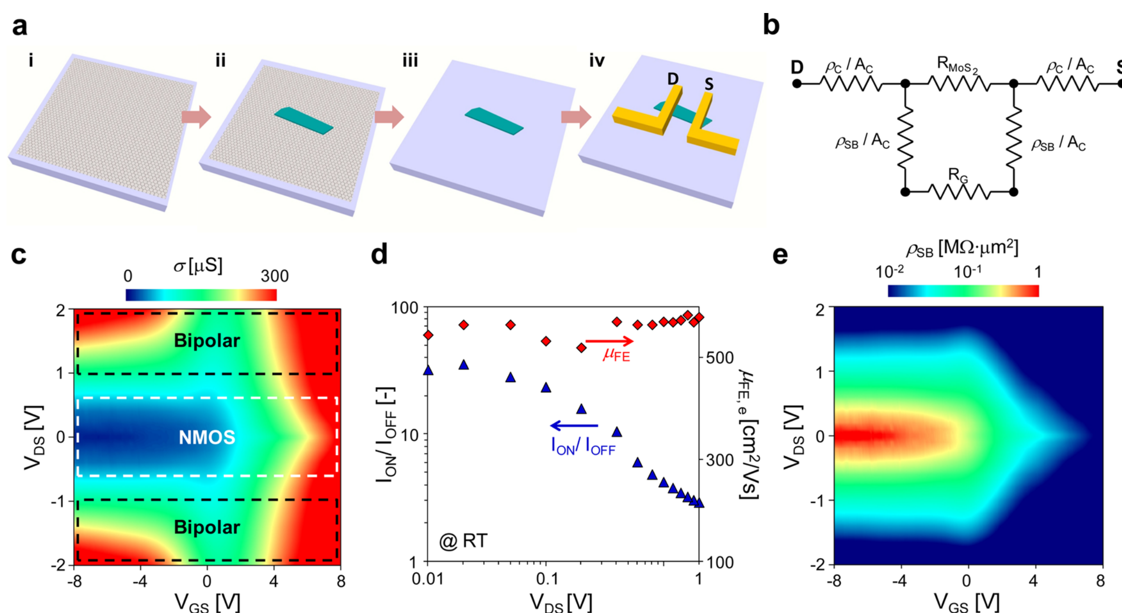

Figure 3. Electronic transport in an MoS_2–graphene heterostructure. (a) Schematic illustration of the fabrication process of the proposed FET device architecture composed of an MoS_2–graphene heterostructure. (b) Simplified equivalent circuit diagram for the FET device considered. (c) Measured transport characteristics for a trilayer MoS_2–graphene FET device ($A_C \sim$ 12 μm^2) as a function of V_{GS} and V_{DS} at room temperature. (d) Measured on/off current ratio I_{ON}/I_{OFF} and electron field-effect mobility $\mu_{FE,e}$ as a function of V_{DS}. (e) Calculated interlayer impedance ρ_{SB} as a function of V_{DS} and V_{GS} at room temperature.

simplified using the equivalent circuit diagram shown in Figure 3b. As a result, the total device conductivity, σ, is given by

$$\sigma = \frac{1}{2\rho_C/A_C + R_{Channel}} \sim \frac{1}{R_{Channel}} = \frac{1}{R_{MoS_2}} + \frac{1}{2\rho_{SB}/A_C + R_G} \sim \frac{1}{2\rho_{SB}/A_C + R_G} \quad (1)$$

where ρ_C is the contact resistivity between MoS_2 and the S/D electrodes, A_C is the S/D contact area, $R_{Channel}$ is the channel resistance, ρ_{SB} is the resistivity of the atomic Schottky barrier formed between MoS_2 and graphene, and R_{MoS_2} and R_G correspond to the resistances of MoS_2 and graphene in the channel region, respectively. It is noteworthy that eq 1 is valid under the following assumptions: (i) $\rho_C/A_C \ll R_{Channel}$, and (ii) $R_{MoS_2} \gg R_G$, which are generally valid. The equation clearly suggests that the transport characteristics in the heterostructure will be determined by the competition between ρ_{SB}/A_C and R_G, depending on the applied gate and drain voltages. The transport characteristics as a function of gate (V_{GS}) and drain (V_{DS}) voltages for a representative thin (~3-layer, Δ = 22.5 cm^{-1}, $A_C \sim$ 12 μm^2, see Figure S7, Supporting Information) MoS_2–graphene FET device are shown in Figure 3c. The measured resistivities (1/G) for the heterostructure considered as a function of V_{GS} under different V_{DS} are shown in Figure S8 (Supporting Information). The calculated field-effect electron mobility for the device is about 600 cm^2/(V s) at room temperature, which is close to that in our CVD graphene device on SiO_2 substrate (see Figure S5, Supporting Information), suggesting that MoS_2 does not scatter electronic transport in graphene significantly, while the defects formed during graphene synthesis limit the transport. We expect that if the single-crystalline graphene (*e.g.*, the "Scotch-tape" graphene) is considered in this structure, the mobility may be affected by the adjacent MoS_2 layer. The mobility value, nevertheless, is significantly higher than that in our MoS_2-only devices (~25 cm^2/(V s), which is comparable to the reported values;[25,26] see Figure S6, Supporting Information). The transport curves at a high drain-source bias, V_{DS}, (*e.g.*, V_{DS} = 1.5 V) regime exhibit bipolar behavior, suggesting that the transport is mainly graphene-controlled (*i.e.*, $R_G \gg \rho_{SB}/A_C$). The minimum conductivity, which is located at $V_{GS} \sim 1$ V, corresponds to the CNP of graphene in the heterostructure, confirming its slightly hole-doped nature, as we indicated in the previous section. In the low V_{DS} regime, since V_{DS} becomes comparable to the Schottky barrier height formed when $V_{GS} < V_{CNP}$, the significant increase of interlayer impedance results in NMOS digital characteristics (*i.e.*, $R_G \ll \rho_{SB}/A_C$), which suggests that the transport of holes in graphene is significantly depleted. Note that since the contact resistivity between MoS_2 and S/D electrodes, ρ_C, (see eq 1) is independent of V_{GS},[24] one can estimate ρ_C from the transport characteristics at the bipolar regime (V_{DS} > 1 V and V_{GS} > 5 V), which yields the value of ~10^{-3}–10^{-2} MΩ μm^2, justifying the assumption of $\rho_C/A_C \ll R_{Channel}$ used to simplify eq 1.

The gate-controlled interlayer impedance enables "NMOS digital" transport in the heterostructure in the low V_{DS} regime, as shown in Figure 3d (characterized at room temperature and V_{GS} = 1.0 V). Since the interlayer

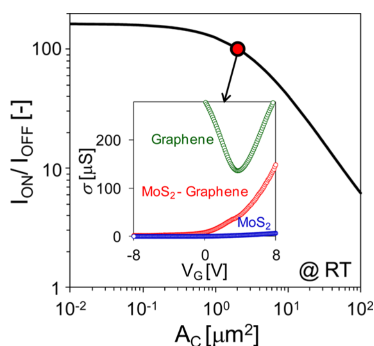

Figure 4. Engineering on/off current ratio in the MoS_2–graphene FET device considered by tuning the contact area A_C. Calculated I_{ON}/I_{OFF} at room temperature and V_{DS} = 10 mV as a function of A_C. The inset corresponds to the calculated transport curve for A_C = 1 μm^2 (red). The measured transport curves for our representative MoS_2 (blue) and graphene (green) FET devices are also shown for comparison.

impedance becomes negligible when $V_{GS} \gg V_{CNP}$, the field-effect mobility of electrons ($\mu_{FE,e}$) in graphene is not affected. However, the significant increase in ρ_{SB} when $V_{GS} < V_{CNP}$ results in a reduction of off current, as well as of the on/off current ratio for the device. For the device considered here, an on/off current ratio of 36 is obtained for $V_{DS} \sim 0.1$ V at room temperature, which is, to our knowledge, the highest value ever reported in monolayer graphene-based FET devices, without sacrificing the field-effect mobility of graphene at the "on" state. To further quantify the interlayer impedance, ρ_{SB}, it was calculated as a function of V_G and V_D using the measured transport characteristics (Figure 3c) and the proposed eq 1, as shown in Figure 3e. As indicated above, the Schottky barrier height becomes more significant in the regime of $V_{GS} < V_{CNP}$ and small V_{DS}, contributing to a drastic increase in ρ_{SB}. Compared to the typical contact resistivity between metal and graphene,[44] the atomistic Schottky barrier can provide about 1000 times higher impedance in this regime, maintaining an Ohmic contact outside the regime. The calculated ρ_{SB} formed between a piece of 6-layer MoS_2 crystal and graphene is shown in Figure S9 (Supporting Information), which suggests an enlarged high ρ_{SB} regime for thicker MoS_2, enabling a wider range for "digital" operation.

The Schottky barriers formed between MoS_2 and graphene indeed suggest a route toward engineering graphene-based digital FET devices using the heterostructure. One possible approach, for example, is to reduce the contact area, A_C. Specifically, because of the transition for the heterostructure from Schottky to Ohmic behaviors with increasing V_G, the rectifying effect for the term, ρ_{SB}/A_C, in eq 1 can be significantly magnified by reducing A_C. On the basis of the calculated ρ_{SB} (see Figure 3e), the calculated on/off current ratio as a function of A_C is shown in Figure 4. A higher on/off current ratio of ~100 can be further achieved at room temperature using a reasonable contact area ($A_C \sim 1\ \mu m^2$; see the red curve in the inset of Figure 4). The feasible range of V_{DS} for NMOS digital operation, on the other hand, can be tuned by the thickness of MoS_2, as suggested in Figure S9 (Supporting Information). The unique dependence of the transport characteristics on V_{GS}, V_{DS}, and the thickness of MoS_2 enables a controllable transition from NMOS digital to bipolar behaviors, which may be useful for analogue applications as well. To this end, the development of large-area, layer-controlled synthesis of MoS_2 films[45−48] is essential to realize large-scale production using well-developed semiconductor process technology.

CONCLUSIONS

In conclusion, we have investigated charge transfer, photoluminescence, and gate-controlled electronic transport in the junction between two 2D materials: MoS_2 and graphene. Without applying any transverse electric fields, our c-AFM and Raman characterizations show that there is a significant number of electrons transferred from MoS_2 to graphene because of their work function difference. The charge transfer also results in the formation of a Schottky barrier at the interface, increasing interlayer impedance between the two materials. We presume that the built-in potential in the Schottky barrier can split the photoexcited electron–hole pairs in monolayer MoS_2 and significantly reduce its photoluminescence. We fabricated FET devices composed of the MoS_2–graphene heterostructure and showed that the interlayer impedance can be further manipulated by the gate and drain voltages, demonstrating a new type of FET device, which enables a controllable transition from NMOS digital to bipolar characteristics. We report a very high room temperature on/off current ratio ($I_{ON}/I_{OFF} \sim 36$) in comparison to graphene-based FET devices without sacrificing the field-effect electron mobilities in graphene. By engineering the source/drain contact area, we further estimate that a higher value of I_{ON}/I_{OFF} up to 100 can be obtained. We believe that the manipulation of electronic transport and optoelectronic response in 2D materials-based heterostructures, as well as the development of graphene-based digital electronics, will be greatly facilitated by the new 2D heterostructure and device architecture presented here.

Conflict of Interest: The authors declare no competing financial interest.

Acknowledgment. M. S. Strano acknowledges funding from the 2009 U.S. Office of Naval Research Multi University Research Initiative (ONR-MURI) on Graphene Advanced Terahertz Engineering (GATE) at MIT, Harvard, and Boston University. D. Blankschtein and M. S. Strano are grateful for the financial support from the National Science Foundation CBET-1133813. C. J. Shih is grateful for partial financial support from the Chyn Duog Shiah memorial Fellowship awarded by Massachusetts Institute of Technology.

Supporting Information Available: Details of graphene synthesis and transfer, Raman spectroscopy and c-AFM system, and fabrication of MoS_2–graphene heterostructure.

This material is available free of charge *via* the Internet at http://pubs.acs.org.

REFERENCES AND NOTES

1. Wang, Q. H.; Kalantar-Zadeh, K.; Kis, A.; Coleman, J. N.; Strano, M. S. Electronics and Optoelectronics of Two-Dimensional Transition Metal Dichalcogenides. *Nat. Nanotechnol.* **2012**, *7*, 699–712.
2. Wang, H.; Yu, L. L.; Lee, Y. H.; Shi, Y. M.; Hsu, A.; Chin, M. L.; Li, L. J.; Dubey, M.; Kong, J.; Palacios, T. Integrated Circuits Based on Bilayer MoS_2 Transistors. *Nano Lett.* **2012**, *12*, 4674–4680.
3. Yoon, Y.; Ganapathi, K.; Salahuddin, S. How Good Can Monolayer MoS_2 Transistors Be?. *Nano Lett.* **2011**, *11*, 3768–3773.
4. Dimitrakopoulos, C. D.; Mascaro, D. J. Organic Thin-Film Transistors: A Review of Recent Advances. *IBM J. Res. Dev.* **2001**, *45*, 11–27.
5. Geim, A. K.; Novoselov, K. S. The Rise of Graphene. *Nat. Mater.* **2007**, *6*, 183–191.
6. Chen, J. H.; Jang, C.; Xiao, S. D.; Ishigami, M.; Fuhrer, M. S. Intrinsic and Extrinsic Performance Limits of Graphene Devices on SiO_2. *Nat. Nanotechnol.* **2008**, *3*, 206–209.
7. Bolotin, K. I.; Sikes, K. J.; Jiang, Z.; Klima, M.; Fudenberg, G.; Hone, J.; Kim, P.; Stormer, H. L. Ultrahigh Electron Mobility in Suspended Graphene. *Solid State Commun.* **2008**, *146*, 351–355.
8. Dean, C. R.; Young, A. F.; Meric, I.; Lee, C.; Wang, L.; Sorgenfrei, S.; Watanabe, K.; Taniguchi, T.; Kim, P.; Shepard, K. L.; Hone, J. Boron Nitride Substrates for High-Quality Graphene Electronics. *Nat. Nanotechnol.* **2010**, *5*, 722–726.
9. Bae, S.; Kim, H.; Lee, Y.; Xu, X. F.; Park, J. S.; Zheng, Y.; Balakrishnan, J.; Lei, T.; Kim, H. R.; Song, Y. I.; *et al.* Roll-to-Roll Production of 30-Inch Graphene Films for Transparent Electrodes. *Nat. Nanotechnol.* **2010**, *5*, 574–578.
10. Lin, Y. M.; Valdes-Garcia, A.; Han, S. J.; Farmer, D. B.; Meric, I.; Sun, Y. N.; Wu, Y. Q.; Dimitrakopoulos, C.; Grill, A.; Avouris, P.; *et al.* Wafer-Scale Graphene Integrated Circuit. *Science* **2011**, *332*, 1294–1297.
11. Novoselov, K. S.; Fal'ko, V. I.; Colombo, L.; Gellert, P. R.; Schwab, M. G.; Kim, K. A Roadmap for Graphene. *Nature* **2012**, *490*, 192–200.
12. Taychatanapat, T.; Jarillo-Herrero, P. Electronic Transport in Dual-Gated Bilayer Graphene at Large Displacement Fields. *Phys. Rev. Lett.* **2010**, *105*, 166601.
13. Shih, C.-J.; Wang, Q. H.; Jin, Z.; Paulus, G. L. C.; Blankschtein, D.; Jarillo-Herrero, P.; Strano, M. S. Disorder Imposed Limits of Mono- and Bilayer Graphene Electronic Modification Using Covalent Chemistry. *Nano Lett.* **2013**, *13*, 809–817.
14. Mak, K. F.; Lee, C.; Hone, J.; Shan, J.; Heinz, T. F. Atomically Thin MoS_2: A New Direct-Gap Semiconductor. *Phys. Rev. Lett.* **2010**, *105*, 136805.
15. Han, S. W.; Kwon, H.; Kim, S. K.; Ryu, S.; Yun, W. S.; Kim, D. H.; Hwang, J. H.; Kang, J. S.; Baik, J.; Shin, H. J.; Hong, S. C. Band-Gap Transition Induced by Interlayer Van Der Waals Interaction in MoS_2. *Phys. Rev. B: Condens. Matter Mater. Phys.* **2011**, *84*, 045409.
16. Ayari, A.; Cobas, E.; Ogundadegbe, O.; Fuhrer, M. S. Realization and Electrical Characterization of Ultrathin Crystals of Layered Transition-Metal Dichalcogenides. *J. Appl. Phys.* **2007**, *101*, 014507.
17. Radisavljevic, B.; Radenovic, A.; Brivio, J.; Giacometti, V.; Kis, A. Single-Layer MoS_2 Transistors. *Nat. Nanotechnol.* **2011**, *6*, 147–150.
18. Kim, S.; Konar, A.; Hwang, W. S.; Lee, J. H.; Lee, J.; Yang, J.; Jung, C.; Kim, H.; Yoo, J. B.; Choi, J. Y.; *et al.* High-Mobility and Low-Power Thin-Film Transistors Based on Multilayer MoS_2 Crystals. *Nat. Commun.* **2012**, *3*, 1011.
19. Li, H.; Yin, Z. Y.; He, Q. Y.; Li, H.; Huang, X.; Lu, G.; Fam, D. W. H.; Tok, A. I. Y.; Zhang, Q.; Zhang, H. Fabrication of Single- and Multilayer MoS_2 Film-Based Field-Effect Transistors for Sensing NO at Room Temperature. *Small* **2012**, *8*, 63–67.
20. Yin, Z. Y.; Li, H.; Li, H.; Jiang, L.; Shi, Y. M.; Sun, Y. H.; Lu, G.; Zhang, Q.; Chen, X. D.; Zhang, H. Single-Layer MoS_2 Phototransistors. *ACS Nano* **2012**, *6*, 74–80.
21. Liu, H.; Ye, P. D. D. MoS_2 Dual-Gate Mosfet with Atomic-Layer-Deposited Al_2O_3 as Top-Gate Dielectric. *IEEE Electron Device Lett.* **2012**, *33*, 546–548.
22. Qiu, H.; Pan, L. J.; Yao, Z. N.; Li, J. J.; Shi, Y.; Wang, X. R. Electrical Characterization of Back-Gated Bi-Layer MoS_2 Field-Effect Transistors and the Effect of Ambient on Their Performances. *Appl. Phys. Lett.* **2012**, *100*, 123104.
23. Lee, K.; Kim, H. Y.; Lotya, M.; Coleman, J. N.; Kim, G. T.; Duesberg, G. S. Electrical Characteristics of Molybdenum Disulfide Flakes Produced by Liquid Exfoliation. *Adv. Mater.* **2011**, *23*, 4178–4181.
24. Das, S.; Chen, H.-Y.; Penumatcha, A. V.; Appenzeller, J. High Performance Multilayer MoS_2 Transistors with Scandium Contacts. *Nano Lett.* **2012**, *13*, 100–105.
25. Fuhrer, M. S.; Hone, J. Measurement of Mobility in Dual-Gated MoS_2 Transistors. *Nat. Nanotechnol.* **2013**, *8*, 146–147.
26. Radisavljevic, B.; Kis, A. Mobility Engineering and a Metal-Insulator Transition in Monolayer MoS_2. *Nat. Mater.* **2013**, *12*, 815–820.
27. Yang, H.; Heo, J.; Park, S.; Song, H. J.; Seo, D. H.; Byun, K. E.; Kim, P.; Yoo, I.; Chung, H. J.; Kim, K. Graphene Barristor, a Triode Device with a Gate-Controlled Schottky Barrier. *Science* **2012**, *336*, 1140–1143.
28. Yu, W. J.; Li, Z.; Zhou, H.; Chen, Y.; Wang, Y.; Huang, Y.; Duan, X. Vertically Stacked Multi-Heterostructures of Layered Materials for Logic Transistors and Complementary Inverters. *Nat. Mater.* **2013**, *12*, 246–252.
29. Britnell, L.; Gorbachev, R. V.; Jalil, R.; Belle, B. D.; Schedin, F.; Mishchenko, A.; Georgiou, T.; Katsnelson, M. I.; Eaves, L.; Morozov, S. V.; *et al.* Field-Effect Tunneling Transistor Based on Vertical Graphene Heterostructures. *Science* **2012**, *335*, 947–950.
30. Necas, D.; Klapetek, P. Gwyddion: An Open-Source Software for Spm Data Analysis. *Cent. Eur. J. Phys.* **2012**, *10*, 181–188.
31. Shi, Y.; Zhou, W.; Lu, A.-Y.; Fang, W.; Lee, Y.-H.; Hsu, A. L.; Kim, S. M.; Kim, K. K.; Yang, H. Y.; Li, L.-J.; *et al.* Van Der Waals Epitaxy of MoS_2 Layers Using Graphene as Growth Templates. *Nano Lett.* **2012**, *12*, 2784–2791.
32. Malard, L. M.; Pimenta, M. A.; Dresselhaus, G.; Dresselhaus, M. S. Raman Spectroscopy in Graphene. *Phys. Rep.* **2009**, *473*, 51–87.
33. Das, A.; Pisana, S.; Chakraborty, B.; Piscanec, S.; Saha, S. K.; Waghmare, U. V.; Novoselov, K. S.; Krishnamurthy, H. R.; Geim, A. K.; Ferrari, A. C.; *et al.* Monitoring Dopants by Raman Scattering in an Electrochemically Top-Gated Graphene Transistor. *Nat. Nanotechnol.* **2008**, *3*, 210–215.
34. Wang, Q. H.; Jin, Z.; Kim, K. K.; Hilmer, A. J.; Paulus, G. L. C.; Shih, C. J.; Ham, M. H.; Sanchez-Yamagishi, J. D.; Watanabe, K.; Taniguchi, T.; *et al.* Understanding and Controlling the Substrate Effect on Graphene Electron-Transfer Chemistry *via* Reactivity Imprint Lithography. *Nat. Chem.* **2012**, *4*, 724–732.
35. Lee, C.; Yan, H.; Brus, L. E.; Heinz, T. F.; Hone, J.; Ryu, S. Anomalous Lattice Vibrations of Single- and Few-Layer MoS_2. *ACS Nano* **2010**, *4*, 2695–2700.
36. Ferrari, A. C.; Meyer, J. C.; Scardaci, V.; Casiraghi, C.; Lazzeri, M.; Mauri, F.; Piscanec, S.; Jiang, D.; Novoselov, K. S.; Roth, S.; *et al.* Raman Spectrum of Graphene and Graphene Layers. *Phys. Rev. Lett.* **2006**, *97*, 187401.
37. Mak, K. F.; He, K.; Lee, C.; Lee, G. H.; Hone, J.; Heinz, T. F.; Shan, J. Tightly Bound Trions in Monolayer MoS_2. *Nat. Mater.* **2013**, *12*, 207–211.
38. Nair, R. R.; Blake, P.; Grigorenko, A. N.; Novoselov, K. S.; Booth, T. J.; Stauber, T.; Peres, N. M. R.; Geim, A. K. Fine Structure Constant Defines Visual Transparency of Graphene. *Science* **2008**, *320*, 1308.
39. Bernardi, M.; Palummo, M.; Grossman, J. C. Extraordinary Sunlight Absorption and One Nanometer Thick Photovoltaics Using Two-Dimensional Monolayer Materials. *Nano Lett.* **2013**, *13*, 3664–3670.

40. Zhang, W.; Chuu, C.-P.; Huang, J.-K.; Chen, C.-H.; Tsai, M.-L.; Chang, Y.-H.; Liang, C.-T.; Chen, Y.-Z.; Chueh, Y.-L.; He, J.-H.; *et al.* Ultrahigh-Gain Photodetectors Based on Atomically Thin Graphene-MoS_2 Heterostructures. *Sci. Rep.* **2014**, *4*, 3826.
41. Buscema, M.; Steele, G. A.; Zant, H. S. J. v. d.; Castellanos-Gomez, A. The Effect of the Substrate on the Raman and Photoluminescence Emission of Atomically Thin MoS_2. Arxiv: 1311.3869, **2013**.
42. Park, J. K.; Song, S. M.; Mun, J. H.; Cho, B. J. Graphene Gate Electrode for MoS Structure-Based Electronic Devices. *Nano Lett.* **2011**, *11*, 5383–5386.
43. Sze, S. M.; Ng, K. K. *Physics of Semiconductor Devices*, 3rd ed.; Wiley-Interscience: Hoboken, NJ, 2007.
44. Venugopal, A.; Colombo, L.; Vogel, E. M. Contact Resistance in Few and Multilayer Graphene Devices. *Appl. Phys. Lett.* **2010**, *96*, 013512.
45. Lee, Y.-H.; Zhang, X.-Q.; Zhang, W.; Chang, M.-T.; Lin, C.-T.; Chang, K.-D.; Yu, Y.-C.; Wang, J. T.-W.; Chang, C.-S.; Li, L.-J.; *et al.* Synthesis of Large-Area MoS_2 Atomic Layers with Chemical Vapor Deposition. *Adv. Mater.* **2012**, *24*, 2320–2325.
46. Najmaei, S.; Liu, Z.; Zhou, W.; Zou, X.; Shi, G.; Lei, S.; Yakobson, B. I.; Idrobo, J.-C.; Ajayan, P. M.; Lou, J. Vapour Phase Growth and Grain Boundary Structure of Molybdenum Disulphide Atomic Layers. *Nat. Mater.* **2013**, *12*, 754–759.
47. van der Zande, A. M.; Huang, P. Y.; Chenet, D. A.; Berkelbach, T. C.; You, Y.; Lee, G.-H.; Heinz, T. F.; Reichman, D. R.; Muller, D. A.; Hone, J. C. Grains and Grain Boundaries in Highly Crystalline Monolayer Molybdenum Disulphide. *Nat. Mater.* **2013**, *12*, 554–561.
48. Yu, Y.; Li, C.; Liu, Y.; Su, L.; Zhang, Y.; Cao, L. Controlled Scalable Synthesis of Uniform, High-Quality Monolayer and Few-Layer MoS_2 Films. *Sci. Rep.* **2013**, *3*, 1866.